

# Attentive Contractive Flow: Improved Contractive Flows with Lipschitz-constrained Self-Attention

Avideep Mukherjee<sup>1</sup>, Badri N. Patro<sup>2\*</sup>, Sahil Sidheekh<sup>3</sup>, Maneesh Singh<sup>3</sup>, Vinay P. Namboodiri<sup>4</sup>

<sup>1</sup> Indian Institute of Technology Kanpur, <sup>2</sup> KU Leuven <sup>3</sup> Verisk Analytics, <sup>4</sup> University of Bath  
 avideep@cse.iitk.ac.in, badri.patro@kuleuven.be, i31549@verisk.com, maneesh.singh@verisk.com, vpn22@bath.ac.uk

## Abstract

Normalizing flows provide an elegant method for obtaining tractable density estimates from distributions by using invertible transformations. The main challenge is to improve the expressivity of the models while keeping the invertibility constraints intact. We propose to do so via the incorporation of localized self-attention. However, conventional self-attention mechanisms don't satisfy the requirements to obtain invertible flows and can't be naively incorporated into normalizing flows. To address this, we introduce a novel approach called Attentive Contractive Flow (ACF) which utilizes a special category of flow-based generative models - contractive flows. We demonstrate that ACF can be introduced into a variety of state of the art flow models in a plug-and-play manner. This is demonstrated to not only improve the representation power of these models (improving on the bits per dim metric), but also to results in significantly faster convergence in training them. Qualitative results, including interpolations between test images, demonstrate that samples are more realistic and capture local correlations in the data well. We evaluate the results further by performing perturbation analysis using AWGN demonstrating that ACF models (especially the dot-product variant) show better and more consistent resilience to additive noise.<sup>1</sup>

## 1 Introduction

While deep generative models based on generative adversarial networks (GANs) and variational autoencoders (VAEs) produce state of the art results showing impressive results on mega-pixel images, they do not have the ability to obtain exact likelihood estimates. To address this need, flow based approaches such as real NVP (Dinh, Sohl-Dickstein, and Bengio 2016) and invertible residual networks (Behrmann et al. 2019) have been proposed. However, flow-based models are still limited in their modeling capabilities as compared to GANs and VAEs. This paper focuses on improving the modeling capability of these models through incorporation of self-attention in them. For this purpose, a sub-category of flow-based generative models called contractive flows (Rezende and Mohamed 2015) is leveraged.

The challenge in obtaining effective mappings from a *simple* latent space representation to a *complex* target distribu-

tion lies in maintaining the constraints for a valid normalizing flow: (a) invertibility of the transformation function, and, (b) the tractable computation of the log-determinant of the Jacobian of the transformation function. Unfortunately, attention in normalizing flows can't be naively incorporated while satisfying the above constraints. In this paper, we show that a category of flow-based models, called contractive flows, can be effectively leveraged for incorporating attention while addressing the above needs. Such models, called Attentive Contractive Flows (ACF) are demonstrated to have faster convergence during training, better modeling capability as well as better resilience to noise in the input data.

Learning data distributions has witnessed remarkable success through generative adversarial networks (GANs) such as StyleGAN2 (Karras et al. 2020). Similarly, remarkable progress has been made using hierarchical variational autoencoders and normalizing flows: NVAE (Vahdat and Kautz 2020) and Flow++ (Ho et al. 2019) provide impressive results for generative modeling based on variational autoencoders and normalizing flows, respectively. Flow++ introduces a step where self-attention is applied to a slice of the image in the coupling layer to improve the expressivity of the transformation. However, so far, incorporating attention for the whole image space at a given step in normalizing flow-based models has not been proposed to the best of our knowledge.

Localized importance in the image space and latent space can be achieved by applying the concept of self-attention (Vaswani et al. 2017; Cheng, Dong, and Lapata 2016). Self-attention offers a balance between the ability to model interdependent features and the computational and statistical efficiency. The self-attention module calculates response at a position as a weighted sum of the features at all positions, where the weights – or attention vectors – are calculated with only a small computational cost. Hence, our main motivation is derived from the fact that during density estimation of complex and high dimensional data, it is important to have information about the key positions in the image that is representative of a particular sample, which in turn is obtained through attention. While convolutional neural network does the job of extracting local features from an image and its subsequent feature transformations, having self-attention as an additional building block definitely improves the expres-

<sup>\*</sup>This research was done in IITK

<sup>1</sup>The paper is under consideration at Computer Vision and Image Understanding

sivity of the model. This information not only helps in tasks like image recognition but also proves to be valuable in the area of generative modelling. Self-attention has been incorporated in GANs (Zhang et al. 2019) and VAEs (Lin, Liu, and Liang 2019). However, as Normalizing Flow models have different transformation functions, it is challenging to incorporate self-attention in Normalizing Flows in a generic sense.

A main challenge we need to solve in order to achieve this task is to examine the invertibility of the self-attention module. In this paper we show that while the general self-attention module is not uniquely invertible, a variant of self-attention is possible that satisfies this property by being a contraction. This class of self-attention is incorporated in three different contractive flows: iResNet (Behrmann et al. 2019), Residual Flows (Chen et al. 2019) and iDenseNets (Perugachi-Diaz, Tomczak, and Bhulai 2021) each one being an improvement over the previous one. We show that the performance of all the three contractive flows gets better respectively with Self Attention. A contractive flow uses Banach’s Fixed Point Theorem to guarantee exact iterative inverses of arbitrarily complex neural networks, as long as the neural network function remains a contraction. We use the variant of self-attention mechanism inside a contractive neural network to provide a perfectly law-abiding flow-based generative model. Through this model we are also able to obtain improved expressive capability for obtaining flows and show significantly improved performance with fewer steps as compared to other state-of-the-art NF models.

## 2 Background

### 2.1 Flow-Based Generative Models

Normalizing Flows are a class of generative models where an ‘simple’ parameterizable base distribution is transformed into a more complex approximation for the posterior distribution (Rezende and Mohamed 2015). This transformation is achieved by passing the base distribution through a series of invertible and bijective mappings. Let  $\mathbf{z} \in \mathbb{R}^D$  and  $\mathbf{y} = \mathbf{f}(\mathbf{z})$ . Let  $\mathbf{z} \sim q(\mathbf{z})$ , be a simple base distribution. The change of variables theorem expresses a relation between the probability density functions  $p_Y(\mathbf{y})$  and  $q(\mathbf{z})$ :

$$p_Y(\mathbf{y}) = q(\mathbf{z}) \left| \det \frac{\partial \mathbf{f}^{-1}}{\partial \mathbf{y}} \right| = q(\mathbf{z}) \left| \det \frac{\partial \mathbf{f}}{\partial \mathbf{z}} \right|^{-1} \quad (1)$$

If we apply a series of such mappings  $f_k, k \in 1, \dots, K$  with  $K \in \mathbb{N}_+$ , we obtain a **normalizing flow**. The log probability of the final distribution can thus be obtained by:

$$\log p_Y(\mathbf{y}) = \log p_Y(\mathbf{z}_K) = \log q(\mathbf{z}_0) - \sum_{k=1}^K \log \left| \det \frac{\partial f_k}{\partial \mathbf{z}_{k-1}} \right| \quad (2)$$

From Equation 1 & 2, it is clearly observed that every normalizing flow architecture must satisfy two conditions. First, the transformation function should be invertible. Secondly, the log-determinant of the Jacobian should be tractable.

### 2.2 Contractive Flows

**iResNet & Residual Flows** Residual Flows (Papamakarios et al. 2019) are a class of invertible functions of the form:

$$\mathbf{z}' = \mathbf{f}(\mathbf{z}) = \mathbf{z} + \mathbf{g}_\phi(\mathbf{z}) \quad (3)$$

where  $\mathbf{g}_\phi : \mathbb{R}^D \mapsto \mathbb{R}^D$  is a neural network with parameters  $\phi$ . (Behrmann et al. 2019) proposed the transformation of Equation 3 as an invertible residual network or iResNet. Residual transformations like this can be made invertible with certain constraints on  $\mathbf{g}_\phi$ . (Behrmann et al. 2019) show that a residual transformation is guaranteed to be invertible if the function  $\mathbf{g}_\phi$  is a *contraction*. A *contraction* is a special case of a Lipschitz continuous function. A function  $F : \mathbb{R}^D \mapsto \mathbb{R}^D$  is said to be  $K$ -Lipschitz continuous when for a given distance measure  $\delta$ , there exists a constant  $K$  such that for two inputs  $\mathbf{x}_1$  and  $\mathbf{x}_2$  we have:

$$\delta(F(\mathbf{x}_1), F(\mathbf{x}_2)) \leq K\delta(\mathbf{x}_1, \mathbf{x}_2) \quad (4)$$

The smallest such  $K$  is called the Lipschitz constant of  $F$  or  $\text{Lip}(F)$ . If  $\text{Lip}(F) \leq 1$ , then  $F$  is said to be a *contraction*. Let us consider the following equation involving the contraction in Equation 3.

$$\mathbf{F}(\hat{\mathbf{z}}) = \mathbf{z}' - \mathbf{g}_\phi(\hat{\mathbf{z}}) \quad (5)$$

Since  $\mathbf{g}_\phi$  is contractive,  $\mathbf{F}$  is also contractive with the same Lipschitz constant. Therefore, from *Banach’s Fixed Point Theorem* (Rudin 2006, 1976), it is ensured that there exists a unique  $\mathbf{z}_*$  such that  $\mathbf{z}_* = \mathbf{z}' - \mathbf{g}_\phi(\mathbf{z}_*)$  which can be rearranged to  $\mathbf{z}' = \mathbf{f}(\mathbf{z}_*)$ . Hence it follows that  $\mathbf{f}$  is invertible (Papamakarios et al. 2019). In fact, the inversion algorithm is iteratively designed from Equation 5 as follows:

$$z_{k+1} = z' - \mathbf{g}_\phi(z_k) \quad \text{for } k \geq 0 \quad (6)$$

The Banach’s fixed-point theorem guarantees the convergence of the recursive algorithm at an exponential rate to  $\mathbf{z}_* = \mathbf{f}^{-1}(\mathbf{z}')$  for any arbitrary initialization of  $z_0$  (usually it is preferred to have  $z_0 = z'$ ). It is clearly observed that composition of  $K$  such residual transformations also preserve the contractive properties with Lipschitz constant being  $\prod_{i=1}^K L_K$ , where  $L_K$  is the respective Lipschitz constant of  $F_K$ . However, there are two major challenges to build residual flows. First off, the design of the neural network function is restricted to being Lipschitz continuous, that too contractive which limits the flexibility of the network. Secondly, the calculation of log-determinant of the Jacobian of such a transformation cannot be efficiently computed except for automatic differentiation which takes  $\mathcal{O}(D^3)$  time. However, the log-determinant can be approximated using the results of (Hall 2015) and (Withers and Nadarajah 2010) and re-written as a power series of the trace of the Lipschitz network  $\mathbf{g}_\phi$ :

$$\begin{aligned} \log |\det J_{f_\phi}(\mathbf{z})| &= \log |\det (\mathbf{I} + J_{g_\phi}(\mathbf{z}))| \\ &= \sum_{k=1}^{\infty} \frac{(-1)^{k+1}}{k} \text{Tr} \{ J_{g_\phi}^k(\mathbf{z}) \} \end{aligned} \quad (7)$$

where  $J_{g_\phi}^k(\mathbf{z})$  is the  $k$ -th power of the Jacobian of  $\mathbf{g}_\phi$  at  $\mathbf{z}$ . The trace can be estimated using Hutchinson trace estimator (Hutchinson 1989). **Residual Flows** (Chen et al. 2019) improved this method where the power series can be finitely approximated using the unbiased Russian-roulette estimator. This results in lower requirement of computation of the power series than in case of iResNet. Also, they introduce LipSwish activation function to avoid derivative saturation.

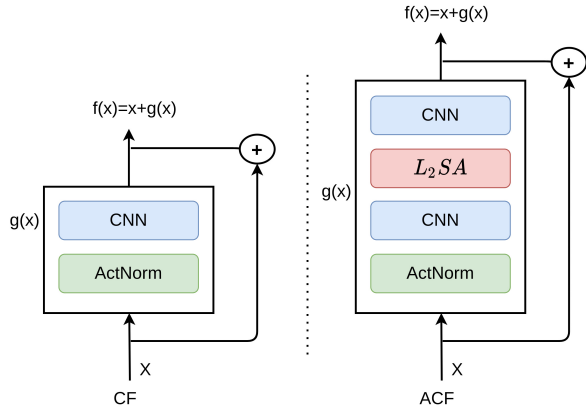


Figure 1: Model diagram comparing one step of the transformation function of a generic contractive flow (CF) (left) and a contractive flow with Self Attention (ACF)(right). SA stands for Self Attention.

**Invertible DenseNets** Invertible DenseNets (Perugachi-Diaz, Tomczak, and Bhulai 2021) use a DenseBlock as a residual layer. A DenseBlock in iDenseNet is slightly different than a standard DenseBlock and is defined as  $F : \mathbb{R}^d \mapsto \mathbb{R}^d$  with  $F(x) = x + g(x)$  where  $g$  is comprised of dense layers  $\{h_i\}_{i=i}^{n+1}$ .  $h_{n+1}$  is a  $1 \times 1$  convolution to match the dimension of the output size  $\mathbb{R}^d$ . Each  $h_i$  has two concatenated parts, the input and the transformed input:

$$h_i(x) = \begin{bmatrix} x \\ \phi(W_i(x)) \end{bmatrix} \quad (8)$$

where  $W_i$  is convolutional matrix and  $\phi$  is a non-linearity with  $\text{Lip}(\phi) \leq 1$  such as ReLU, ELU, LipSwish (Chen et al. 2019) or CLipSwish (Perugachi-Diaz, Tomczak, and Bhulai 2021).

### 3 Method: Contractive Flows with Self-Attention

Before defining the transformation function with self-attention, we need to make sure that the two conditions of normalizing flow function are satisfied i.e, the function is invertible and the log-determinant of the Jacobian is tractable. In order to have attention incorporated in contractive flows, the attention module needs to be inserted in between the convolutional layers in the function  $g_\phi$  of Equation 3. This would require the attention function to be a Lipschitz continuous function. Since the attention function involves computing a dot-product between the query and key matrices, it will be referred to as *dot-product self-attention*. Even if the dot-product self-attention module can be inverted, the log-determinant of the Jacobian is hard to compute. A trick to compute non-tractable log-determinant of the Jacobian is to use the results of (Withers and Nadarajah 2010) that reduces computing the determinant to computing the trace. The result shows that for any non-singular matrix  $A \in \mathbb{R}^{d \times d}$

$$\ln(\det A) = \text{tr}(\ln A)$$

where  $\ln$  is a matrix logarithm,  $\text{tr}$  is the trace of a matrix. However, this result requires the determinant be a positive

quantity. It is proven that the Lipschitz constrained perturbations of the form  $x + g(x)$  yield positive Jacobian determinants (Behrmann et al. 2019). Therefore, for a function  $F(x) = x + g(x)$ , we have,

$$|\det J_F(x)| = \det J_F(x) \quad (9)$$

Here comes the role of contractive flows which defines transformation functions as  $F(x) = x + g(x)$ . But, as explained in Section 2.2, in order to make the transformation function invertible,  $g$  should not only be Lipschitz continuous but also needs to be a *contraction*, i.e.,  $\text{Lip}(g) < 1$ . The traditional self-attention function that is popular in different architectures like Transformers (Vaswani et al. 2017) or Self-Attention GANs (Zhang et al. 2019) is not Lipschitz continuous (Kim, Papamakarios, and Mnih 2020). Fortunately, there's an alternative formulation of the self-attention function given by Kim *et al.* (Kim, Papamakarios, and Mnih 2020) that is proven to be Lipschitz continuous. The traditional Self Attention was referred as dot-product Self Attention and the alternative was called  $L_2$  Self Attention, since the expression replaces computation of the dot product between the key and value convolutions with an  $L_2$  Norm. The expressions of the  $L_2$  Self Attention are provided keeping in mind a multi-headed Self Attention module that is most commonly prevalent in several transformer architectures. In this work, since the attention mechanism is to be applied over images and not text, we have considered the number of heads to be one and have modified the equations of (Kim, Papamakarios, and Mnih 2020) in the following way. The  $L_2$  self-attention function on an image  $X \in \mathbb{R}^{N \times D}$  (where  $N$  is the product of the height and width of the image and  $D$  is the number of channels) replaces the dot-product operation performed in dot-product self-attention module by:

$$P_{i,j} \propto \exp(L_{i,j}) = \exp\left(-\frac{\|x_i^T W^Q - x_j^T W^K\|_2^2}{\sqrt{D}}\right) \quad (10)$$

Here  $W^Q = W^K \in \mathbb{R}^{D \times \bar{D}}$ . This is necessary for the function to be Lipschitz as proven in (Kim, Papamakarios, and Mnih 2020). So, the full attention-mechanism function is:

$$F(X) = P X A W^V W^O \quad (11)$$

where,  $W^O, W^V \in \mathbb{R}^{D \times D}$ ,  $A = W^Q (W^K)^T / \sqrt{D} \in \mathbb{R}^{D \times D}$  and  $P \in \mathbb{R}^{N \times N}$  is given by with the normalization constant that makes sure that  $\sum_j P_{i,j} = 1$ . Since there is no non-linear activation function involved between  $W^V$  and  $W^O$  in the expression of Equation 11, the product of the two  $1 \times 1$  convolution matrices can be replaced by a single one. Hence, the equation can be further simplified to:

$$F(X) = P X A W^L \quad (12)$$

where  $W^L$  is a  $1 \times 1$  convolution matrix which acts as a replacement parameter of  $W^V W^O$ . Substituting  $W^V W^O$  by  $W^L$  reduces the number of parameters significantly and in turn makes the training process time and memory efficient. Also, since the second dimension of  $W^Q$ , i.e.  $\bar{D}$  gets dissolved in multiplication, we can replace it by  $\frac{D}{k}$  for  $k = 1, 2, 4, 8, \dots$ . We have used  $\bar{D} = \frac{D}{8}$  for memory efficiency. Equation 10 can be rewritten using matrix operations

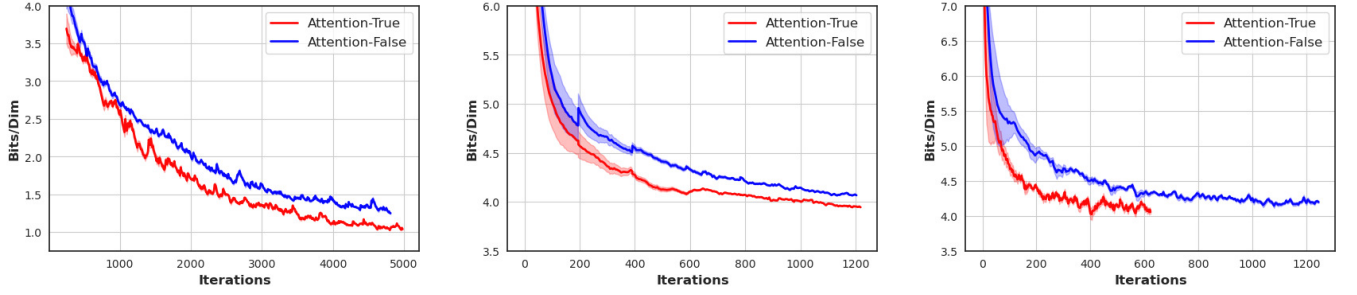


Figure 2: Convergence plots on (a) iResNet on MNIST, (b) Residual Flows on CIFAR10 and (c) Invertible DenseNet on ImageNet32, in terms of train bits/dim across iterations. We observe that contractive flows with Self Attention converge faster (even with fewer steps of the flow) than their non-attention counterparts.

**Algorithm 1:** Pseudo Code for a forward pass of an ACF. SN stands for Spectral Normalization as in (Behrmann et al. 2019)

---

**Input:** network  $f$ , residual block  $g$ , number of power series terms  $n$ ,  $W^Q$ : the query convolution,  $W^V$ ,  $W^O$ : the value and out convolution respectively

**Data:**  $X \in \mathbb{R}^{N \times D}$  (where  $N$  is the product of the height and width of the image and  $D$  is the number of channels)

---

```

1 for each residual block do
2   Lip constraint:  $\hat{W}_j := SN(W_j, X)$  for Layer  $W_j$ 
3    $P :=$ 
4      $S \left( - \frac{\|XW^Q\|_r^2 \mathbf{1}^T - 2XW^Q(XW^Q)^T + \mathbf{1}\|XW^Q\|_r^{2T}}{\sqrt{D}} \right)$ 
5   Replacement Matrix:  $W^L := W^V \times W^O$  as in eq: 12
6    $A := W^Q(W^Q)^T / \sqrt{D}$ 
7    $F := P \times X \times A \times W^L$  as in eq: 11
8    $Lip_2(F) :=$ 
9      $\frac{\sqrt{N}}{\sqrt{D}} (4\phi^{-1}(N-1) + 1) \|W^Q\|_2 \|W^V\|_2 \|W^O\|_2$ 
10   $W_{j+1} := \gamma \frac{F}{Lip_2(F)} + X$ : the final attention output as mentioned in eq: 15
11  Draw  $v$  from  $\mathcal{N}(0, \mathbf{I})$ 
12   $w^T = v^T$ 
13   $\ln \det := 0$ 
14  for  $k = 1$  to  $n$  do
15     $w^T := w^T J_g$  (vector-Jacobian product)
16     $\ln \det := \ln \det + (-1)^{k+1} w^T v / k$ 

```

---

for efficient computation as:

$$P = S \left( - \frac{\|XW^Q\|_r^2 \mathbf{1}^T - 2XW^Q(XW^Q)^T + \mathbf{1}\|XW^Q\|_r^{2T}}{\sqrt{D}} \right) \quad (13)$$

where  $S$  is the softmax function and  $\|A\|_r^2$  indicates the squared  $L_2$  norm to each row of  $A$ , so if  $A \in \mathbb{R}^{m \times n}$ , then  $\|A\|_r^2 \in \mathbb{R}^m$ . This formulation of self-attention, also known as the  $L_2$  Self-Attention is proven to be Lipschitz continuous with the following bound on  $Lip_2(F)$ :

$$Lip_2(F) \leq \frac{\sqrt{N}}{\sqrt{D}} (4\phi^{-1}(N-1) + 1) \|W^Q\|_2 \|W^V\|_2 \|W^O\|_2 \quad (14)$$

where  $\phi(x) = x \exp(x + 1)$  is an invertible univariate function on  $x > 0$  and  $N$  is the input size. Also,  $\phi^{-1}(N-1) = W_0(\frac{N}{e})$  where  $W_0$  is the Lambert W-function (Kim, Papamakarios, and Mnih 2020). Hence, in order to make  $F$  a contraction, we divide  $F$  by the upper bound of  $Lip_2(F)$  to obtain contractive- $L_2$  Self-Attention. This function satisfies every property of being a part of the transformation function of the normalizing flow. Therefore, final attention output is given by:

$$\text{out} = \gamma \frac{F}{Lip_2(F)} + X \quad (15)$$

where  $\gamma$  is a learnable scalar initialized to 0.  $\gamma$  helps the network to first attend to the local features in the neighborhood and then gradually learn to assign more weight to the non-local evidence (Zhang et al. 2019). A detailed procedure of the forward pass of one step of the flow along with the computation of the  $L_2$  Self Attention is provided in Algorithm 1.

## 4 Experiments

We evaluated the inclusion of Self Attention in three different contractive flows: invertible ResNets, Residual Flows, and invertible DenseNets. Quantitative analysis includes comparison with other state-of-the-art methods using the popular bits/dim metric (Table 1) on various datasets as discussed in section 4.1. We analyze the rate of convergence of the flows both with and without attention and discuss them in Figure 2. The qualitative analysis includes visualizations for the reconstruction of real images as well as generated samples (Figure 3). Further, we also interpolate between latent variables to demonstrate that ACF helps achieve smooth transitions between samples in the image space (Figure 4). Finally, we conduct ablation studies to validate the robustness and efficacy of ACF.

### 4.1 Datasets

To experimentally validate the efficacy of ACF, we consider the datasets - MNIST (LeCun and Cortes 2010), CIFAR10 (Krizhevsky, Nair, and Hinton 2014), ImageNet32 and ImageNet64 (Chrabaszcz, Loshchilov, and Hutter 2017). Due to constrained resources we could not conduct experiments on higher-dimensional datasets like CelebA HQ 256. However, we conduct experiments on a down-sampled version of



Model	MNIST	CIFAR 10	IMAGE NET32	IMAGE NET64
Real NVP	1.06	3.49	4.28	3.98
Glow	1.05	3.35	4.09	3.81
FFJORD	0.99	3.40	-	-
Flow++	-	3.29	3.86*	3.69*
iResNet (iR)	1.05	3.45	-	-
iR + SA (ACF)	<b>0.87</b>	3.40	-	-
ResFlow (RF)	0.97	3.28	4.01	3.76
RF + SA (ACF)	0.92	3.34	3.86	<b>3.70</b>
iDenseNet (iD)	-	3.25	3.98	-
iD + SA (ACF)	-	<b>3.14</b>	<b>3.75</b>	-

Table 1: Results [bits/dim] on standard benchmark datasets for density estimation. \* are the results obtained through variational dequantization (Ho et al. 2019) which we do not compare against (following Residual Flow).

the CelebA-HQ dataset ( 5bit  $64 \times 64$ ) and provide qualitative results. We follow the standard train-test split for each of these datasets, as further elaborated below. The CIFAR10 dataset consists of 60,000  $32 \times 32$  color images belonging to 10 classes, with 6000 images per class. We train the models on 50,000 images and keep the rest 10,000 images to generate the test results. The MNIST dataset contains 70,000  $28 \times 28$  black and white images belonging to 10 classes, each class signifying a digit. We use 60,000 for the training of the models and the remaining 10,000 images for testing. The ImageNet32 and ImageNet64 datasets each comprise 1,281,167 training images from 1000 classes and 50,000 test images (50 images per class). The 5bit CelebA-HQ64 dataset contains 202,599 face images and is pre-processed as defined in (Papamakarios et al. 2019).

## 4.2 Density Estimation and Generative Modeling

We train the attentive contractive flow models (iResNet+SA, Residual Flow+SA, iDenseNet+SA) on the datasets reported in their non-attentive counterparts (section 5.1). We also follow the same architecture for each of these models, except for the addition of the self-attention layer within each transformation block. Specifically, the models follow a multi-scale architecture with multiple blocks of invertible transformation and Self Attention incorporated into them. A diagram of how each attentive block compares with the non-attentive counterpart is provided in Figure 1. Though the block-wise architectures are similar, the added expressivity provided by self-attention enables us to use fewer no. of transformation blocks in ACF, all the while attaining superior performance. We summarize the density estimation results for ACF quantitatively using the test bits/dim metric in Table 1, comparing it with the non-attentive contractive flows as well as other state-of-the-art models. We observe that ACF not only helps improve contractive flows but also outperforms the other state-of-the-art results. Further, ACF also complements the lift in performance with a faster convergence rate (Figure 2). Despite using fewer transfor-

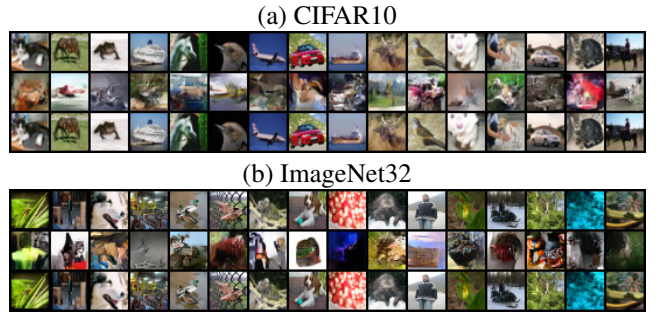


Figure 3: The images in the top, bottom and middle row are respectively the real, reconstructed and generated images. (a) CIFAR10 results from ACF (Residual Flows). (b) ImageNet32 results from ACF (iDenseNet).



Figure 4: Interpolation between CelebA images, from one face to another using ACF(Residual Flow) and Eq.- 16.

mation blocks, ACF trained for a smaller no. of epochs is able to outperform (on average) its non-attentive counterparts. For example, the ACF results shown (Table 1) are generated from models that have been trained for fewer than 100 epochs, whereas the numbers reported in iResNet (Behrmann et al. 2019), Residual Flows (Chen et al. 2019), and Invertible DenseNets (Perugachi-Diaz, Tomczak, and Bhulai 2021) are from models that underwent 200-300 epochs of training for all the datasets. This empirically validates the added expressivity of ACF. In all our experiments, we use the log determinant approximation that is usually followed in various contractive flows and also briefly described in Section 2.2. Further model-specific architectures and implementation details are provided in the supplementary material.

## 4.3 Qualitative Results

Figure 3 depicts qualitative samples and reconstructed images for ACF(Residual Flow) and ACF(iDenseNet) on CIFAR10 and ImageNet32. We observe that ACF is able to obtain exact reconstructions as well as generate realistic samples. Further qualitative samples reconstructions and samples on different datasets are provided in the supplementary

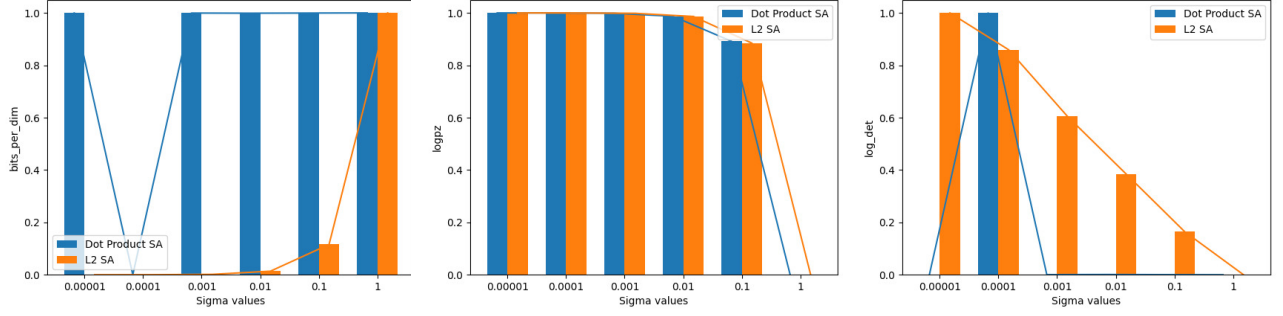


Figure 5: Variation of (a)bits/dim, (b)log likelihood and (c) volume correction values in ACF with dot-product and ACF with  $L_2$  Self Attention with the change in intensity of Gaussian noises applied to perturb the input MNIST images. While the variations in the values with  $L_2$  Self Attention are always consistent, the dot-product plots again fail to produce such consistent variations.

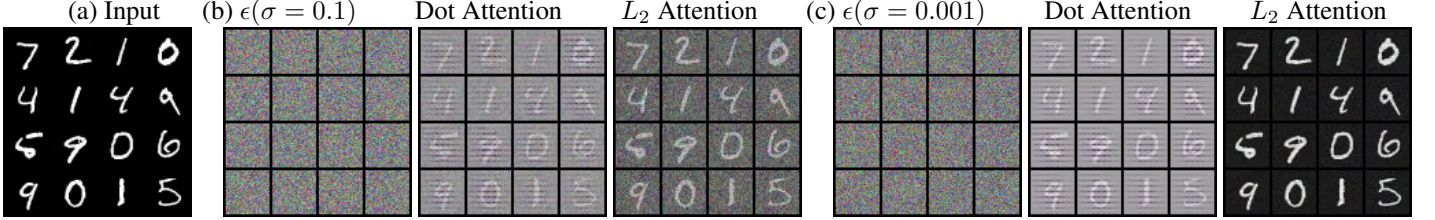


Figure 6: Reconstructions of perturbed input images by a Contractive Flow with Dot and  $L_2$  Self Attention. The perturbation is done by adding Gaussian noises ( $\epsilon$ ) of different variances ( $\sigma$ ) as shown in (b) and (c). ACF with  $L_2$  Self Attention produces better reconstructions with decrease in the intensity of noise. ACF with dot-product Self Attention fails to do so.

material.

We also train ACF(Residual Flow) on the CelebA dataset and perform interpolation between test images to provide a better visual intuition. We apply the transformation function (trained ACF) on the test images and obtain the corresponding samples in the latent space, i.e., the simple base distribution. We then perform linear interpolation between random pairs of images in the latent space, obtaining  $N$  equally spaced interpolated latent samples per pair. We then apply the inverse of the transformation function on the interpolated latent samples to obtain their corresponding images. More formally, the input images, say  $x_1$  and  $x_2$  are passed through the forward transformation function of the model to generate the random variables from the simple distribution, say  $z_1$  and  $z_2$ . The intermediate random variables are generated by the following incremental operation:

$$\delta = z_1 + \frac{i}{N} \times (z_2 - z_1) \quad \forall i \in \{0, 1, 2, \dots, N+1\} \quad (16)$$

We follow the increment rule provided in the computation of integrated gradients (Sundararajan, Taly, and Yan 2017). The procedure to generate the interpolated reconstructions is described in Algorithm 2. The results are depicted in Figure 4. We observe that ACF is able to interpolate effectively, providing smooth transitions between pairs of diverse and unseen faces. Further interpolation results are provided in the supplementary material.

#### Algorithm 2: Interpolation Between Two Images

**Input:**  $f$ : model,  $nSteps$ : interpolation steps)

**Data:**  $x_{C_1}$  and  $x_{C_2}$

- 1  $z_{C_1} = f(x_{C_1})$  and  $z_{C_2} = f(x_{C_2})$
- 2 **for**  $i \in \{0, 1, 2, \dots, nSteps + 1\}$  **do**
- 3      $\delta = z_{C_1} + \frac{i}{nSteps} \times (z_{C_2} - z_{C_1})$   
       reconstructed\_image =  $f^{-1}(\delta)$

Noise ( $\sigma$ )	ACF(dot-product)	ACF( $L_2$ )
0.1	-726.63	42889.64
0.01	35772.76	4959.88
0.001	-9298.64	512.88
0.0001	-15126.88	47.50

Table 2: Comparison of bits/dim of reconstructions of the perturbed input images with Gaussian noises with the corresponding variances on ACF with dot-product Self Attention and ACF with  $L_2$  Self Attention.

#### 4.4 Perturbation Analysis with Gaussian Noise

We perform ablations to study the robustness of Attentive Contractive Flows and validate the need for  $L_2$  Self Attention over dot-product Self Attention by qualitatively and quantitatively evaluating the reconstructions of perturbed input images. For this experiment, we consider ACF(iResNet) over the MNIST dataset. The input images are perturbed

by adding Gaussian noises of different variances( $\sigma$ ) - 0.00001, 0.0001, 0.001, 0.01, 0.1, 1. We quantitatively evaluate the model by reporting the bits/dim values of the reconstructions for the different levels of noises. We compare the performance of  $L_2$  Self Attention based ACF with dot product Self Attention based ACF in Table 2. The fact that dot-product self attention is not Lipschitz constrained leads to wrongful computation of the log-probability using the change of variable formula which sometime results in negative bits/dim as we can see in Table 2. On the other hand, we observe that the model with  $L_2$  Self Attention performs better and more consistently. The qualitative results in Figure 6 also demonstrate that the reconstructions for ACF( $L_2$ ) improve with decreasing values of  $\sigma$ . However, such is not the case with dot-product Self Attention. The robustness of using  $L_2$  Self Attention with ACF is also graphically demonstrated in Figure 5(a),(b) and (c). While ACF with  $L_2$  Self Attention follows the natural and consistent increase in bits/dim, dot product Self Attention fails to perform as expected and produces random undesirable values. We notice similar behavioral consistencies w.r.t the change in the trace values and also the log probability values when  $L_2$  SA is used instead of dot-product SA.

## 5 Related Works

We provide an overview of the main related works in the following areas.

### 5.1 Attention in generative models

Deep generative modeling has drawn significant research interest in recent years, and many state-of-the-art techniques have emerged. The objective is to estimate the density or the distribution of the data and generate new samples from the estimated distribution. This estimation can either be done implicitly or explicitly, giving rise to varied approaches. Perhaps the most famous among models that do implicit density estimation is GANs (Goodfellow et al. 2014), which revolutionized the field of image synthesis and slowly found applications in different modes of generative modeling. A GAN effectively poses the unsupervised task of data generation as a supervised learning problem through an adversarial min-max game between two agents; A generator that maps a latent space to the data space and a discriminator that learns to distinguish the real data samples from the fake samples that the generator produces. Self Attention GAN (Zhang et al. 2019) incorporates the self-attention mechanism on both the generator and discriminator of a GAN, establishing competitive results.

In the domain of explicit density estimation, the density is either approximated or tractably estimated. Variational autoencoders (VAEs) constitute the most famous example among approximate density estimation models, apart from Boltzmann Machines (Smolensky 1986). VAEs explicitly optimize the log-likelihood of the data by maximizing the evidence lower bound (ELBO) (Kingma and Welling 2013). Assuming the data distribution to be Gaussian, the objective function tries to find the best parameters that fit the data. A recent work proposes to incorporate Self Attention on the

encoder feature space of VAEs, to enable a better approximation of the posterior (Lin, Liu, and Liang 2019).

### 5.2 Normalizing Flows

In our work, we focus on normalizing flow models. They are a class of generative models that aims to estimate a tractable density of the data. Other popular approaches in this domain include fully visible belief networks like NADE (Uria et al. 2016), MADE (Kumar et al. 2016), PixelCNN, PixelRNN (Oord, Kalchbrenner, and Kavukcuoglu 2016; Van den Oord et al. 2016) and WaveNet (Oord et al. 2016). Normalizing Flows (Rezende and Mohamed 2015) fall under the category broadly known as change of variable models, which employ the theorem to transform a simple parameterizable base distribution into some complex approximation of the posterior distribution. In contrast to GANs and VAEs, normalizing flows are an attractive class due to their ability to obtain tractable density estimates. Prominent normalizing flow models include Non-Linear Independent Components Estimation (NICE) (Dinh, Krueger, and Bengio 2014), real non-volume preserving (real NVP) flow (Dinh, Sohl-Dickstein, and Bengio 2016), inverse autoregressive flow (IAF) (Kingma et al. 2016), masked autoregressive flow (MAF) (Papamakarios, Pavlakou, and Murray 2017), and Glow (Kingma and Dhariwal 2018).

Flow++ (Ho et al. 2019) suggests technical and implementation tweaks for designing powerful normalizing flow models. One of the suggestions is to use Self Attention in the affine coupling layers of models such as real NVP (Dinh, Sohl-Dickstein, and Bengio 2016). However, the model only provides attention to a slice of the image or feature space at any given step instead of the whole image. Hence, while using Self Attention in a part of the input improves the performance marginally, we provide a way to incorporate Self Attention into normalizing flows in such a way that the attention is applied to the whole image and feature spaces at once instead of just a slice, thereby improving the performance of the normalizing flow models by a greater margin.

## 6 Conclusion

Through this work, we present a principled method for incorporating self-attention into contractive flows for modeling complex image distributions. The addition of global self-attention, i.e., self-attention on the whole image/transformed feature space, helps improve the expressivity of normalizing flows. We establish, through exhaustive experimentation, that  $L_2$  self-attention helps attain state-of-the-art results while driving faster model convergence. Interesting future directions to explore include understanding how/why self-attention helps improve specific model architectures better than others. We believe that our contributions open new avenues for research to strengthen the representative power of normalizing flows, bringing principled, efficient, and tractable density estimation a step closer.

## References

Behrmann, J.; Grathwohl, W.; Chen, R. T.; Duvenaud, D.; and Jacobsen, J.-H. 2019. Invertible residual networks. In

- International Conference on Machine Learning*, 573–582.
- Chen, R. T.; Behrmann, J.; Duvenaud, D. K.; and Jacobsen, J.-H. 2019. Residual flows for invertible generative modeling. In *Advances in Neural Information Processing Systems*, 9916–9926.
- Cheng, J.; Dong, L.; and Lapata, M. 2016. Long short-term memory-networks for machine reading. *arXiv preprint arXiv:1601.06733*.
- Chrabaszcz, P.; Loshchilov, I.; and Hutter, F. 2017. A Down-sampled Variant of ImageNet as an Alternative to the CIFAR datasets. *arXiv:1707.08819*.
- Dinh, L.; Krueger, D.; and Bengio, Y. 2014. Nice: Non-linear independent components estimation. *arXiv preprint arXiv:1410.8516*.
- Dinh, L.; Sohl-Dickstein, J.; and Bengio, S. 2016. Density estimation using real nvp. *arXiv preprint arXiv:1605.08803*.
- Goodfellow, I.; Pouget-Abadie, J.; Mirza, M.; Xu, B.; Warde-Farley, D.; Ozair, S.; Courville, A.; and Bengio, Y. 2014. Generative adversarial nets. In *Advances in neural information processing systems*, 2672–2680.
- Hall, B. 2015. *Lie groups, Lie algebras, and representations: an elementary introduction*, volume 222. Springer.
- Ho, J.; Chen, X.; Srinivas, A.; Duan, Y.; and Abbeel, P. 2019. Flow++: Improving flow-based generative models with variational dequantization and architecture design. *arXiv preprint arXiv:1902.00275*.
- Hutchinson, M. F. 1989. A stochastic estimator of the trace of the influence matrix for Laplacian smoothing splines. *Communications in Statistics-Simulation and Computation*, 18(3): 1059–1076.
- Karras, T.; Laine, S.; Aittala, M.; Hellsten, J.; Lehtinen, J.; and Aila, T. 2020. Analyzing and Improving the Image Quality of StyleGAN. *2020 IEEE/CVF Conference on Computer Vision and Pattern Recognition (CVPR)*.
- Kim, H.; Papamakarios, G.; and Mnih, A. 2020. The Lipschitz Constant of Self-Attention. *arXiv preprint arXiv:2006.04710*.
- Kingma, D. P.; and Dhariwal, P. 2018. Glow: Generative flow with invertible 1x1 convolutions. In *Advances in neural information processing systems*, 10215–10224.
- Kingma, D. P.; Salimans, T.; Jozefowicz, R.; Chen, X.; Sutskever, I.; and Welling, M. 2016. Improved variational inference with inverse autoregressive flow. In *Advances in neural information processing systems*, 4743–4751.
- Kingma, D. P.; and Welling, M. 2013. Auto-encoding variational bayes. *arXiv preprint arXiv:1312.6114*.
- Krizhevsky, A.; Nair, V.; and Hinton, G. 2014. The cifar-10 dataset. *online: <http://www.cs.toronto.edu/kriz/cifar.html>*, 55.
- Kumar, A.; Irsoy, O.; Ondruska, P.; Iyyer, M.; Bradbury, J.; Gulrajani, I.; Zhong, V.; Paulus, R.; and Socher, R. 2016. Ask me anything: Dynamic memory networks for natural language processing. In *International conference on machine learning*, 1378–1387.
- LeCun, Y.; and Cortes, C. 2010. MNIST handwritten digit database.
- Lin, L.; Liu, X.; and Liang, W. 2019. Improving Variational Auto-Encoder with Self-Attention and Mutual Information for Image Generation. In *Proceedings of the 3rd International Conference on Video and Image Processing, ICVIP 2019*, 162–167. New York, NY, USA: Association for Computing Machinery. ISBN 9781450376822.
- Oord, A. v. d.; Dieleman, S.; Zen, H.; Simonyan, K.; Vinyals, O.; Graves, A.; Kalchbrenner, N.; Senior, A.; and Kavukcuoglu, K. 2016. Wavenet: A generative model for raw audio. *arXiv preprint arXiv:1609.03499*.
- Oord, A. v. d.; Kalchbrenner, N.; and Kavukcuoglu, K. 2016. Pixel recurrent neural networks. *arXiv preprint arXiv:1601.06759*.
- Papamakarios, G.; Nalisnick, E.; Rezende, D. J.; Mohamed, S.; and Lakshminarayanan, B. 2019. Normalizing flows for probabilistic modeling and inference. *arXiv preprint arXiv:1912.02762*.
- Papamakarios, G.; Pavlakou, T.; and Murray, I. 2017. Masked autoregressive flow for density estimation. In *Advances in Neural Information Processing Systems*, 2338–2347.
- Perugachi-Diaz, Y.; Tomczak, J. M.; and Bhulai, S. 2021. Invertible densenets with concatenated lipswish. *arXiv preprint arXiv:2102.02694*.
- Rezende, D. J.; and Mohamed, S. 2015. Variational inference with normalizing flows. *arXiv preprint arXiv:1505.05770*.
- Rudin, W. 1976. International series in pure and applied mathematics. *Principles of mathematical analysis*.
- Rudin, W. 2006. *Real and complex analysis*. Tata McGraw-hill education.
- Smolensky, P. 1986. Information processing in dynamical systems: Foundations of harmony theory. Technical report, Colorado Univ at Boulder Dept of Computer Science.
- Sundararajan, M.; Taly, A.; and Yan, Q. 2017. Axiomatic attribution for deep networks. In *International Conference on Machine Learning*, 3319–3328. PMLR.
- Uria, B.; Côté, M.-A.; Gregor, K.; Murray, I.; and Larochelle, H. 2016. Neural autoregressive distribution estimation. *The Journal of Machine Learning Research*, 17(1): 7184–7220.
- Vahdat, A.; and Kautz, J. 2020. NVAE: A Deep Hierarchical Variational Autoencoder. *arXiv preprint arXiv:2007.03898*.
- Van den Oord, A.; Kalchbrenner, N.; Espeholt, L.; Vinyals, O.; Graves, A.; et al. 2016. Conditional image generation with pixelcnn decoders. In *Advances in neural information processing systems*, 4790–4798.
- Vaswani, A.; Shazeer, N.; Parmar, N.; Uszkoreit, J.; Jones, L.; Gomez, A. N.; Kaiser, Ł.; and Polosukhin, I. 2017. Attention is all you need. In *Advances in neural information processing systems*, 5998–6008.
- Withers, C. S.; and Nadarajah, S. 2010.  $\log \det A = \text{tr} \log A$ . *International Journal of Mathematical Education in Science and Technology*, 41(8): 1121–1124.



Zhang, H.; Goodfellow, I.; Metaxas, D.; and Odena, A. 2019. Self-attention generative adversarial networks. In *International Conference on Machine Learning*, 7354–7363. PMLR.

# Supplementary Material for Attentive Contractive Flow: Improved Contractive Flows with Lipschitz-constrained Self-Attention

## Abstract

We provide some additional details and results of our work in this supplementary material. Appendix A includes information about the implementation of the experiments and setup and the hyperparameters chosen. We provide some results about the generated samples and also show some more examples of interpolation between two real images in Appendix B.

## A Implementation and Hyperparameter Details

The ACF models were experimented on the following datasets. Below are the details of the implementation and the hyper-parameters used. For all the experiments except ACF(iResNet) on CIFAR10, data parallelization has been performed. Tables 1, 2 and 3 provide details about the model architecture as well as the experimental environment it was trained in. The **Time** column in the tables refer to time taken per epoch and is calculated as the product of the number of batches of the dataset and the time taken to train each batch.

## B Qualitative Examples

Figure 1 and 2 show some more results from ACF models on various datasets. Figure 3 presents a qualitative comparison on the CelebA dataset between residual flow and ACF (Residual Flow). It can be visually observed that adding attention to the normalizing flow steps contribute in generation of better samples. Interpolations between different CelebA face images while keeping the intermediate generations realistic are demonstrated in Figure 4.

Dataset	Steps	Epochs	Batch Size	#GPU	GPU Type	Time/Epoch (hr)
MNIST	10	120	16	1	TITAN X - 12GB	6.2
CIFAR10	10	110	16	1	TITAN X - 12GB	8.5

Table 1: Implementation and Hyperparameter details on the respective datasets for ACF (iResNet)

Dataset	Steps	Epochs	Batch Size	#GPU	GPU Type	Time/Epoch (hr)
MNIST	10	120	16	3	1080 Ti - 11GB	4.7
CIFAR10	10	110	16	3	TITAN X - 12GB	3.47
ImageNet32	16	1	16	2	TITAN X - 12 GB	164.6
ImageNet64	32	1	16	4	Tesla V100-16GB	266.91
5-bit CelebA - HQ	8	100	64	4	Tesla V100-16GB	0.58

Table 2: Implementation and Hyperparameter details on the respective datasets for ACF (Residual Flow)

Dataset	Steps	Epochs	Batch Size	#GPU	GPU Type	Time/Epoch (hr)
CIFAR10	16	50	32	4	Tesla V100-16GB	9.55
ImageNet32	32	2	32	4	Tesla V100-16GB	207.59

Table 3: Implementation and Hyperparameter details on the respective datasets for ACF (iDenseNet)

(a) CIFAR10



(b) ImageNet32



(c) ImageNet64



(d) 5-bit CelebA HQ



Figure 1: (a,b,c) The images in the top, bottom and middle row are respectively the real, reconstructed and generated images from ACF (Residual Flow). (d) The top two rows represent the read images, the bottom two rows represent their reconstruction and the middle two rows are the generated samples from ACF (Residual Flow).



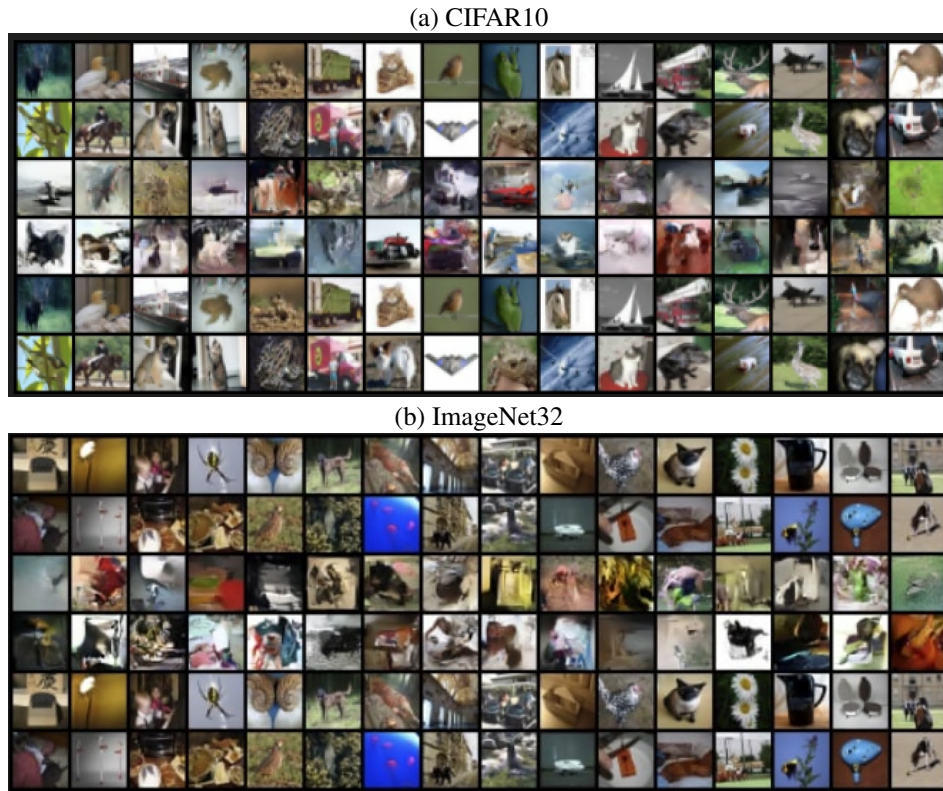


Figure 2: Examples on CIFAR10 (above) and ImageNet32 (below) dataset from ACF(iDenseNet). For each dataset, the top two rows represent the read images, the bottom two rows represent their reconstruction and the middle two rows are the generated samples from the model.

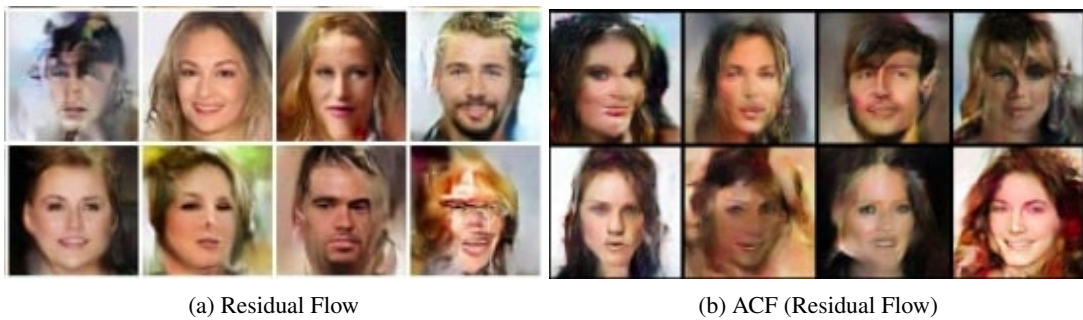


Figure 3: Comparison between CelebA samples generated from vanilla residual flow and ACF (Residual Flow).





Figure 4: Interpolation between CelebA images, from one face to another using ACF(Residual Flow)